Catalysis Science & Technology

Accepted Manuscript

ROYAL SOCIETY OF CHEMISTRY

www.rsc.org/catalysis

Catalysis Science & Technology

PAPER

Ni nanoparticles supported on CNTs with excellent activity produced by atomic layer deposition for hydrogen generation from hydrolysis of ammonia borane

Received 00th January 20xx,
Accepted 00th January 20xx

DOI: 10.1039/x0xx00000x

www.rsc.org/catalysis

Jiankang Zhang,[a,b] Chaoqiu Chen,[a]* Wenjun Yan, Feifei Duan,[a] Bin Zhang,[a] Zhe Gao[a] and Yong Qin[a]*

Highly dispersed, uniform Ni nanoparticles with controlled loadings supported on multi-walled carbon nanotubes (CNTs) were synthesized by atomic layer deposition for hydrogen generation from hydrolysis of ammonia borane (AB). The catalytic performance of Ni/CNTs nanocatalysts prepared with varying ALD cycle numbers was investigated for hydrolysis of AB in water. The results show that all the Ni/CNTs nanocatalysts exhibit excellent catalytic activities towards hydrolysis of AB and the Ni/CNTs produced with 200 ALD cycles have the highest hydrogen generation rate, with a total turnover frequency value as high as 26.2 $mol_{H2}{\cdot}mol_{Ni}^{-1}{\cdot}min^{-1}$, which is higher than that of most nickel-based catalysts previously reported in the literature. The hydrolysis completion time and activation energy of AB hydrolysis are 4.5 min and 32.3 $kJ{\cdot}mol^{-1}$, respectively. Furthermore, 2 ALD cycles of Pt doping (only 0.68 wt%) can significantly improve catalytic activity and reusability of Ni/CNTs nanocatalysts due to its promotion effect. Our results suggest that ALD is a promising technique for designing and fabricating efficient, economical non-noble metal nanocatalysts for hydrolysis of AB.

1. Introduction

Hydrogen is a globally accepted alternative and ideal energy carrier to satisfy the increasing demand for efficient and clean energy.[1-3] However, on-board hydrogen storage in large quantities is one of the major technological barriers for its widespread application.[4] Ammonia borane (NH_3BH_3, AB) is considered as one of the most attractive hydrogen storage materials due to its high hydrogen capacity (19.6 wt%), well-behaved solubility/stability in neutral aqueous solutions at room temperature and non-toxicity.[5] Typically, AB can release hydrogen through either pyrolysis or hydrolysis. The former tends to require high temperatures (>80 °C) to release more hydrogen and generally gives a relatively low rate for hydrogen release.[6] In contrast, the later can proceed rapidly and generate three equivalents of hydrogen per mole of AB with suitable catalysts at room temperature (Eq.1),[7] resulting in a controllable and attractive route for the release of hydrogen. So far, many catalyst systems have been tested for the hydrolysis of AB,[8-11] among which platinum shows the highest activity.[11] However, high price and scarcity of noble metals limit their practical applications. In this regard, the development of highly efficient catalysts based on non-precious and abundant metals is of crucial importance for the effective application of AB.[12, 13]

$$NH_3BH_3 + 2H_2O \xrightarrow{Catalyst} NH_4BO_2 + 3H_2 \quad (1)$$

Among non-noble based metal catalysts, Ni-based catalysts have attracted much attention because of their environmental benignity, low cost and good activity in various catalytic reactions, such as hydrogenation processes and reforming reaction, as well as catalytic hydrolysis of AB. Nevertheless, the catalytic activity of Ni-based materials for hydrolysis of AB is low compared to those of noble metal catalysts.[3, 14-22] Therefore, extensive efforts have been devoted to improving their catalytic activities towards the hydrolysis of AB. Sun's group reported a facile synthesis of monodisperse Ni nanoparticles (NPs) with size of 3.2 nm by reducing $Ni(acac)_2$ with borane tributylamine. The as-synthesized Ni NPs exhibited high catalytic activity for the hydrolysis of AB with a total TOF value of 8.8 $mol_{H2}{\cdot}mol_{Ni}^{-1}{\cdot}min^{-1}$.[18] Cao et al. produced nanoporous nickel spheres with very high surface area through an EG-mediated process, which were highly efficient catalysts for the hydrolytic dehydrogenation of AB, with a total TOF value of 19.6 $mol_{H2}{\cdot}mol_{Ni}^{-1}{\cdot}min^{-1}$.[14] More recently, Xu's group developed a sequential chemical vapor deposition (CVD)-reduction method to prepare highly dispersed Ni NPs immobilized by ZIF-8, which show high catalytic activity with a TOF value of 14.2 $mol_{H2}{\cdot}mol_{Ni}^{-1}{\cdot}min^{-1}$.[12] In a subsequent study, Xu and co-workers selected MSC-30 (a commercial porous carbon material with high surface area of 3140 $m^2{\cdot}g^{-1}$ and micropore volume of 1.7 $m^3{\cdot}g^{-1}$) as a support and prepared Ni@MSC-30 catalysts with highly dispersed Ni NPs via the similar method, which gave a TOF value as high as 30.7 $mol_{H2}{\cdot}mol_{Ni}^{-1}{\cdot}min^{-1}$.[3] These studies demonstrated that downsizing Ni particles to nanoscale is an effective method to boost their catalytic

[a] State Key Laboratory of Coal Conversion, Institute of Coal Chemistry, Chinese Academy of Science, Taiyuan 030001, P.R. China, qinyong@sxicc.ac.cn, chenchaoqiu@sxicc.ac.cn.
[b] Graduate University of Chinese Academy of Sciences, Beijing 100039, P.R. China.
Electronic Supplementary Information (ESI) available. See DOI: 10.1039/x0xx00000x

kinetics towards hydrolysis of AB due to the size effect.[23, 24] The catalytic activity of Ni NPs for hydrolysis of AB can be tailored by controlling their sizes and size distribution. Unfortunately, the synthesis of small Ni NPs with a controlled size and a narrow size distribution is still a challenge since small Ni NPs have high surface energy and readily aggregate to form larger NPs, leading to a wide size distribution and poor dispersion, which limit their catalytic activities. CVD technique often results in non-uniform size and/or non-conformal growth in most substrates.[25] Therefore, a general and facile method that can easily control the nucleation and growth of Ni NPs is very desirable for such application.

Atomic layer deposition (ALD) has emerged as a promising tool for the atomically precise design and synthesis of advanced, nanostructured catalysts.[26-28] ALD is a modified CVD technique based on sequential, self-limiting surface reactions of alternately injected gaseous precursors. The self-limiting character of these reactions makes it possible to deposit conformal coatings of thin films and highly dispersed nanoparticles on high aspect ratio and high surface area porous materials. In the past few years, ALD has been successfully used to design and synthesize highly dispersed metal nanoparticle catalysts with precise controlled particle size, composition, and structure including monometallic and bimetallic catalysts. These new catalysts show significant improved catalytic activity and/or selectivity for various catalytic reactions, including methanol oxidation, CO oxidation, and Cinnamaldehyde and nitrobenzene hydrogenation reactions.[27, 29-34] Nevertheless, previous studies mainly focus on designing and synthesizing various noble metal nanocatalysts using ALD. Application of ALD to design and fabricate non-noble metal nanocatalysts used for hydrolysis of AB has not been reported.

Herein, we present a facile ALD approach to synthesize highly dispersed Ni NPs on CNTs for hydrolysis of AB. The catalytic performance of Ni/CNTs nanocatalysts produced with varying ALD cycle numbers was investigated for hydrolysis of AB in water. The results show that all the Ni/CNTs nanocatalysts exhibit excellent catalytic activities towards hydrolysis of the AB and the Ni/CNTs nanocatalysts produced with 200 ALD cycles exhibit the highest TOF value as high as 26.2 $mol_{H2}\cdot mol_{Ni}^{-1}\cdot min^{-1}$, indicating that the Ni/CNTs nanocatalysts prepared by ALD are efficient, economical catalysts for the hydrolysis of AB. Furthermore, the kinetics behavior of AB hydrolysis catalyzed by Ni/CNTs was studied, and the activation energy E_a was also obtained.

2. Experimental

2.1 Chemicals

Analytical reagent grade ammonia borane complex (NH_3BH_3, Sigma Aldrich, 97%), bis(cyclopentadienyl) nickel (Cp_2Ni, Alfa Aesar, 98%), (methylcyclopentadienyl)trimethylplatinum ($MeCpPtMe_3$, Strem Chemicals, 99%) and nitric acid (HNO_3, Beijing Chemical Reagent Co., Ltd, 68 wt %) were utilized as received without further purification. Raw multi-walled CNTs with diameters in the range of 40-60 nm, length of 5-15 μm, purity of 97%, ash level of 3% and specific surface area of 40-70 $m^2\cdot g^{-1}$ were purchased from Shenzhen Nanotech. Port Co., Ltd. Vulcan XC-72 carbon with specific surface area of 240 $m^2\cdot g^{-1}$ was purchased from Cabot Corp., USA, and graphene (510 $m^2\cdot g^{-1}$) was purchased from Institute of Coal Chemistry, Chinese Academy of Sciences. Deionized water was used for all hydrolysis experiments.

2.2 Catalyst synthesis

Firstly, raw CNTs were pretreated with HNO_3 (68 wt %) for 6 h at 120 °C in an oil bath to remove the amorphous carbon and open the ends of the CNTs, and then washed by deionized water until no further change of pH (around pH = 7). After that, the samples were further washed by anhydrous ethanol, and then filtered. Finally, the functionalized CNTs were dried at 100 °C for 12 h in the oven.

Prior to ALD, the functionalized CNTs were dispersed in ethanol by ultrasonic agitation, dropped onto a quartz wafer, and dried in air. NiO nanoparticles were deposited onto CNTs using a hot-wall, closed chamber-type ALD reactor and the prepared catalysts was denoted as NiO/CNTs. NiO ALD was performed by sequential exposure of the CNTs to $NiCp_2$ and ozone (O_3) produced using an O_3 generator. Deposition temperature for NiO was 280 ^oC and $NiCp_2$ were maintained at 68 ^oC. Nitrogen was used as the carrier and purge gas. Finally, the obtained NiO/CNTs were transferred into a tubular furnace and then reduced at 375 ^oC under 5% H_2/Ar (50 mL/min) atmosphere for 1.5 h to form metallic nickel catalysts denoted as Ni/CNTs. Similar deposition conditions were applied to obtain Pt nanoparticles except that $MeCpPtMe_3$ were maintained at 60 ^oC.

2.3 Catalyst characterization

The XRD patterns were collected on a Bruker D8 Advance X-ray diffractometer with Cu Kα radiation (λ = 1.540 Å) in the 2θ range from 5^o to 90^o. Transmission electron microscopy (TEM) and high resolution TEM (HRTEM) images were taken with a JEOL-2100F microscope. High-angle annular dark-field scanning TEM (HAADF-STEM) and elemental maps were taken with a Tecnai G^2-F20 microscope. The samples for TEM analysis were prepared by dropping one or two ethanol droplets of the samples onto carbon-coated copper grids and drying at room temperature. Raman spectra were collected with a LabRam HR800 (Horiba Jobin Yvon, Palaiseau, France) spectrometer employing a He-Ne laser with an excitation wavelength of 514 nm. The X-ray photoelectron spectra (XPS) were recorded on an ES-300 photoelectron spectrometer (KRATOS Analytical) with an Al Kα source (1486.6 eV). Temperature programmed reduction (TPR) experiments were carried out in an Auto-Chem 2920 instrument using 50 mg sample under 50 $mL\cdot min^{-1}$ H_2 (10%)/Ar with a heating rate of 10 $^oC\cdot min^{-1}$. The Ni and Pt content of the samples was determined by ICP-OES analysis (Thermo ICAP 6300).

2.4 Catalytic hydrolysis of AB

The catalytic activity of the Ni/CNTs catalysts toward hydrolysis of AB was determined by measuring the rate of hydrogen generation in a typical water-filled gas burette system. Before starting the catalytic activity test, a jacketed round-bottom flask (25 mL) containing a Teflon-coated stir bar was placed on a magnetic stirrer and thermostated to 25 ± 0.5 ^oC. Then a burette filled with water was connected to the reaction flask to measure the volume of hydrogen gas evolved from the reaction. Next, a certain amount of catalysts were dispersed in 10 mL of distilled water in the reaction flask, and 1.5 mmol of AB was added into the flask at 700 rpm stirring rate. The volume of hydrogen gas evolved was measured by recording the displacement of water level every 30 s. The reaction was considered

to cease when no hydrogen generation was observed. For a control experiment, 1.5 mmol AB and 13 mg HNO_3 pretreated CNTs (the same amount as the one used in catalytic activity tests) were dissolved in 10 mL of water at 25 ± 0.5 °C. No hydrogen generation was observed in 12 h, indicating that the HNO_3 pretreated CNTs have no catalytic activity in the hydrolysis of AB.

2.5 Catalyst durability in the hydrolysis of AB

After the hydrogen generation reaction was completed, the Ni/CNTs catalysts were kept in the reaction solution under ambient conditions, and another equivalent of AB (1.5 mmol) was added to the reaction flask after all the hydrogen gas has been removed from the reaction system. The gas generation was monitored by the decline of water level in the burette. The same process was then repeated.

3. Result and discussion

3.1 Catalyst characterization

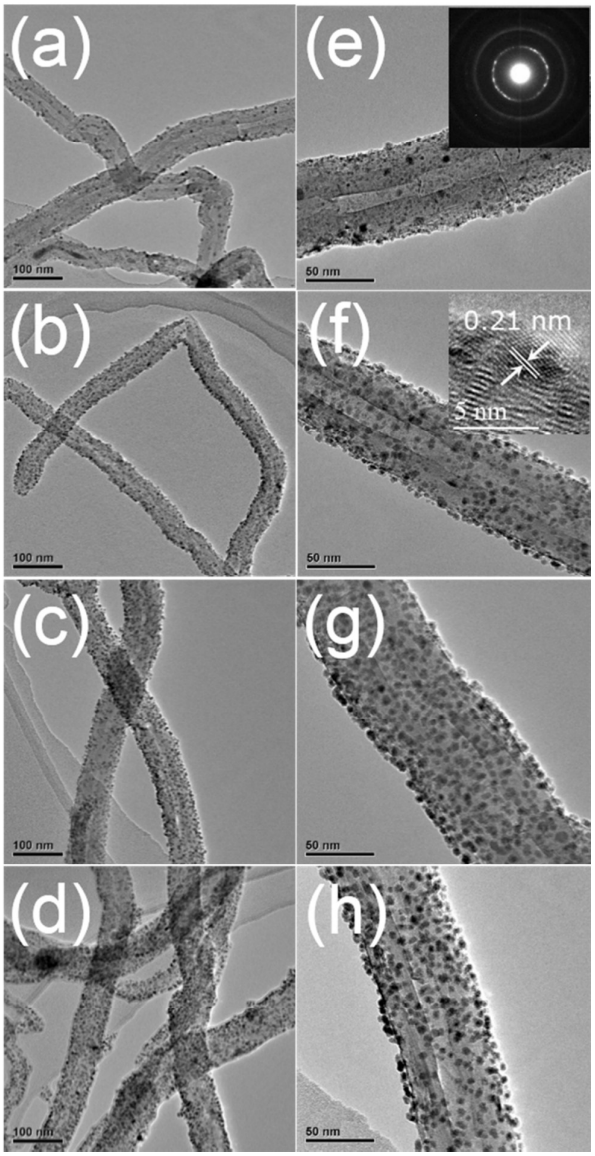

Fig. 1 Low (a, b, c, d) and high magnification (e, f, g, h) TEM images of Ni nanoparticles deposited on CNTs produced by ALD with (a) 50, (b) 100, (c) 200 and (d) 400 ALD cycles respectively followed by hydrogen treatment. The insets of (e) and (f) present the corresponding SAED pattern and HRTEM image, respectively.

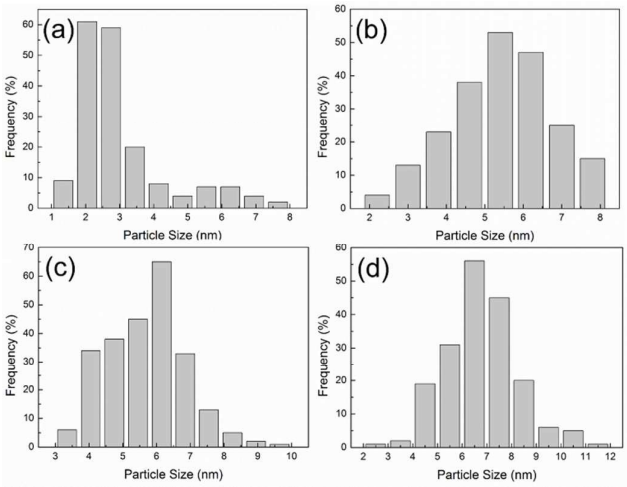

Fig. 2 Histograms of particle size distribution of Ni nanoparticles deposited on CNTs produced by ALD with (a) 50, (b) 100, (c) 200 and (d) 400 ALD cycles respectively followed by hydrogen treatment.

Ni/CNTs nanocatalysts were synthesized by NiO ALD followed by hydrogen treatment. The Ni loading on CNTs can be well controlled by easily varying the number of NiO ALD cycles, yielding 7.22 wt% (50 ALD cycles), 12.63 wt% (100 ALD cycles), 17.22 wt% (200 ALD cycles) and 24.48 wt% (400 ALD cycles) Ni loading, respectively. The morphology and microstructure of the Ni/CNTs nanocatalysts with different Ni loading were examined by TEM, as shown in Fig. 1. It can be seen that all the samples exhibit a uniform dispersion of discrete Ni NPs on the CNTs. The histograms of particle sizes were obtained by measuring more than 200 Ni nanoparticles from multiple images recorded for each sample (Fig. 2). With the increase of Ni loading from 7.22 wt% to 24.48 wt%, the average size of the Ni NPs initially increases and subsequently keeps nearly unchanged (about 3.0 nm, 5.4 nm, 5.6 nm and 5.7 nm, respectively). These results demonstrate that ALD is an effective method to generate highly dispersed Ni NPs on CNTs even with high Ni loading. The corresponding selected area electron diffraction (SAED) pattern (inset in Fig. 1e) shows typical ring patterns, indicating the crystalline nature of the Ni NPs. And this is further confirmed by the X-ray diffraction pattern of the nanoparticles (Fig. 3). HRTEM analysis was conducted to further investigate the crystalline structure of the Ni NPs. The measured distance between adjacent lattice fringes is approximately 0.201 nm, which is consistent with the lattice spacing of the (111) planes of the fcc-Ni.[18]

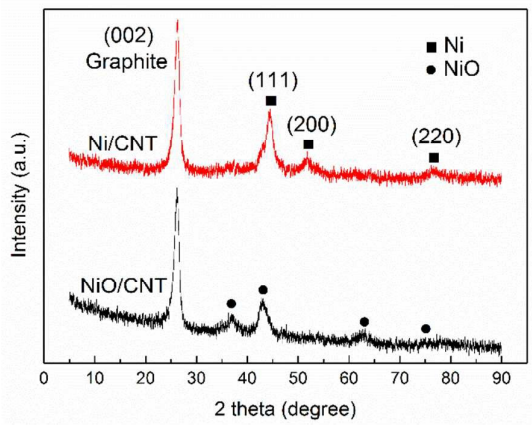

Fig. 3 XRD patterns of the NiO/CNTs and Ni/CNTs catalysts.

To investigate the nickel phase changes on the composites before and after hydrogen treatment, XRD analyses were performed. As shown in Fig. 3, the main diffraction peaks at 2θ = 37.3°, 43.3°, 62.7° and 75.4° relate to the fcc-NiO (JCPDS No.47-1049), and the obvious narrow band located at around 2θ = 26.2° associates to the (002) crystal plane of graphite structure of CNTs.[35] After hydrogen treatment, the nickel phase changes from nickel oxide to metallic nickel, i.e., the main diffraction peaks at 2θ = 44.4°, 51.6° and 76.1° can be readily indexed as (111), (200), and (220) crystal planes of fcc-Ni (JCPDS No.04-0850),[36] which is the active phase for catalytic hydrolysis of AB. The X-ray photoelectron spectroscopy (XPS) measurements were performed to further verify the formation of metallic Ni. XPS survey scan was presented in Fig. S1a in supporting information. C, O and Ni elements are observed from XPS survey spectrum in the samples, conforming the successful deposition of nickel nanoparticles onto CNTs. Metallic Ni peak appears at 852.9 eV for the reduced Ni/CNTs catalysts (Fig. S1b), and the coexistence of oxidized Ni^{2+} in reduced Ni/CNTs catalysts may be attributed to the oxidation during the sample preparation process for the XPS analysis.[37] It should be noted that XPS is mainly a surface analysis technique and probe depth is about ~3 nm for inorganic materials. Thus the relatively strong peak intensity of surface nickel oxide species is detected in the reduced Ni/CNTs catalysts.[43, 44] Another possible reason is that small portion of NiO may not be reduced to metallic Ni^0 under 375 °C due to the strong interaction with support. Moreover, the reduced Ni/CNTs catalysts are magnetically recyclable (Fig. S2), which is convenient for the separation of catalysts from reaction solution during reusability tests.

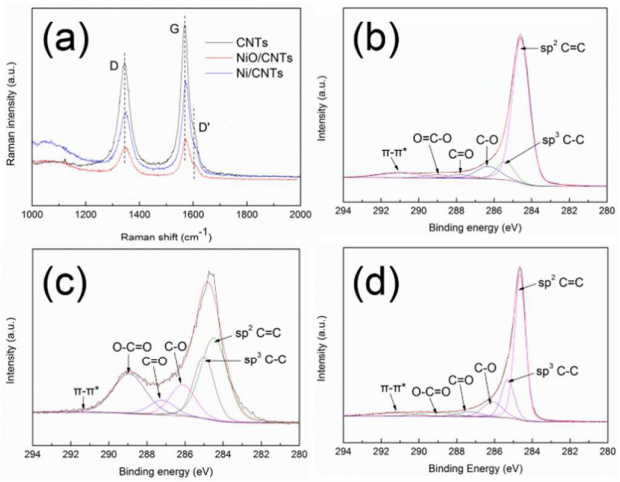

Fig. 4 (a) Raman spectra of CNTs, NiO/CNTs and Ni/CNTs. XPS C1s spectra of (b) CNTs, (c) NiO/CNTs and (d) Ni/CNTs.

Table 1 Raman spectra data of the samples.

Samples	Band position (cm^{-1})		I_D/I_G
	D	G	
CNTs	1344	1569	0.98
NiO/CNTs	1349	1573	1.12
Ni/CNTs	1347	1572	1.00

Fig. 4a shows the Raman spectra of CNTs, NiO/CNTs and Ni/CNTs. Two obvious bands centered around 1344 cm^{-1} (D band) and 1569 cm^{-1} (G band) are the main features of the CNTs for all samples. The small shoulder at around 1606 cm^{-1} is attributed to the D′ band, which is more obvious in NiO/CNTs sample after ALD processing. Both D and G band peaks of NiO/CNTs and Ni/CNTs shift to a higher wavenumber compared with that of CNTs. The value of I_D/I_G is calculated (see table 1) and it is noticeable that this value increases from 0.98 to 1.12 after 200 cycles of NiO ALD, indicating the formation of defects and roughness on CNTs due to the oxidation by ozone during ALD process. This value decreases after hydrogen treatment. O_3 is a strong oxidant and it can create a great amounts of oxygen-containing groups on CNTs support during the ALD process.[38] Fig. 4b-4d show the C1s spectra of CNTs, NiO/CNTs and Ni/CNTs. XPS C1s peak was deconvoluted into six peaks (C=C, C-C, C-O, C=O, O-C=O and π-π*), and the relative content of the functional groups of CNTs, NiO/CNTs and Ni/CNTs was summarized in Table S1. As can be seen from Table S1, the oxygen-containing groups (C-O, C=O, O-C=O) increase obviously after ALD process. And a prominent raised bump at 288.9 eV was observed in the C1s spectra for the NiO/CNTs and this may be ascribed to carboxylate and/or O-COO- functional groups (Fig. 4c),[39] indicating the strong oxidizing capability of ozone toward CNT supports. Moreover, the peak at around 285.1 eV (sp^3 C-C) can be ascribed to defects on the nanotube structure, which corresponds to sp^3-like disorder band (D) at around 1344 cm^{-1} in Raman spectrum.[38] The defect content increases from 9.0% to 21.4% after NiO ALD deposition and then decreases to 17.5% after hydrogen treatment (see Table S1), which is consistent with the Raman results. It is the uniform dispersion of oxygen-containing groups and defects that results in the uniform formation of NiO and Ni NPs on CNTs

support even after the following hydrogen reduction process because those highly dispersive defects and oxygen-containing groups acting as active sites may provide anchoring sites for the nickel precursor chemisorption.[40]

3.2 Catalytic activity of the Ni/CNTs for hydrolysis of AB

The cycle number of NiO ALD has a direct influence on the nanoparticle size and Ni loading, which will further influence hydrogen generation rate. Thus Ni/CNTs catalysts with different Ni loadings were synthesized by varying the number of ALD cycles and their catalytic performance for hydrolysis of AB were investigated in a typical water-filled gas burette system. Fig. 5 shows the amount of H_2 generated as a function of reaction time using different Ni/CNTs nanocatalysts. For all Ni/CNTs samples, a rapid and nearly linear hydrogen evolution was observed after a short introduction period (about 15 s). To directly compare the catalytic activity of the catalysts produced with different ALD cycle numbers, the maximum H_2/AB ratio, completion time, TOF value and the corresponding hydrogen generation rate of Ni/CNTs were evaluated and summarized in Table 2. Obviously, all the four Ni/CNTs samples exhibit good catalytic activity for hydrolysis of AB. And the Ni/CNTs catalysts produced with 200 ALD cycles show the highest catalytic activity, giving a TOF value of 26.2 $mol_{H2}·mol_{Ni}^{-1}·min^{-1}$ and the corresponding hydrogen generation rate is 10720.9 $mL·min^{-1}·g^{-1}$, which are higher than that of most nickel-based catalysts reported previously (shown in Table 3). And it seems that CNT supported nickel catalysts is better than other carbon materials such as XC-72 and graphene in view of the catalytic activity (Fig. S3). Although our present TOF value is slightly lower than the highest TOF value (30.7 $mol_{H2}·mol_{Ni}^{-1}·min^{-1}$) ever reported by Xu's group, our method is very promising as a relatively unexplored approach for the synthesis of metal-based catalysts.[3] Since Ni/CNTs nanocatalyst produced with 200 ALD cycles shows the highest catalytic activity among all the Ni/CNTs nanocatalysts prepared in this work, it is further used to investigate the influence of temperature and catalyst concentration on the hydrolysis of AB in the following kinetics and durability experiments.

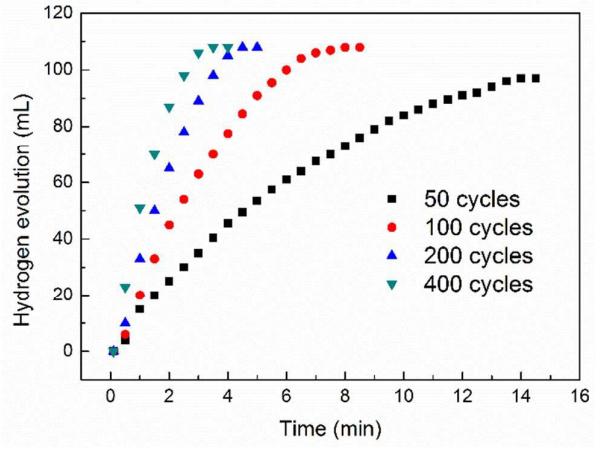

Fig. 5 Hydrogen generation from AB solution (0.15 mol/L, 10.0 mL) at 25 ± 0.5 °C catalyzed by Ni/CNTs (13.0 mg) produced with different ALD cycle numbers.

Table 2 The completion time, TOF value and hydrogen generation rate of Ni/CNTs nanocatalysts produced with different ALD cycle numbers.

Ni/CNTs nanocatalysts produced with different ALD cycle numbers	Completion time (min) [a]	TOF ($mol_{H2}·mol_{Ni}^{-1}·min^{-1}$)	Hydrogen generation rate ($mL·min^{-1}·g^{-1}$)
50	14.5	17.4	7090.5
100	7.5	21.5	8770.3
200	4.5	26.2	10720.9
400	3.5	23.7	9696.1

[a] The corresponding maximum H_2/AB ratio for the Ni/CNTs nanocatalysts is 2.7, 3.0, 3.0 and 3.0 respectively.

Table 3 Catalytic performance of the non-noble nickel-based catalysts catalyst tested in hydrogen generation from the hydrolysis of AB ever reported.

Catalysts	TOF ($mol_{H2}·min^{-1}·mol^{-1}_{Ni}$)	Ref.
Ni/CNTs (200 cycles)	26.2	This work
Ni@MSC-30	30.7	3
Nanoporous Ni spheres	19.6	14
CVD-Ni/ZIF-8	14.2	15
3.2 nm Ni/SiO_2	13.2	17
3.2 nm Ni/C	8.8	18
Starch-stabilized in-site Ni NPs	6.6	19
PVP-stabilized Ni NPs	4.5	20
Hollow-Ni NPs	4.3	21
Ni/γ-Al_2O_3	1.7	22
Ni/C-3	2.0	36

Fig. 6a displays the plot of reaction time versus volume of H_2 generated at different temperatures (20-40 °C). Hydrogen generation rate constant K at these temperatures were obtained by calculating the slope of the fitted linear part of each plot to determine the activation energy E_a. According to the Arrhenius plot of ln k versus $1/T$ (inset of Fig. 6a), E_a is calculated to be about 32.3 $kJ·mol^{-1}$. This value is relatively low, indicating the superior catalytic performance of Ni/CNTs catalysts synthesized by ALD approach. Fig. 6b presents the effect of catalyst concentration on the hydrolysis of AB at 25 ± 0.5 °C. The rates of hydrogen generation rise remarkably with the increase of catalyst concentration under the condition of releasing equivalent H_2. A stoichometric amount of H_2 (~4.5 mmol) was generated within less than 7 min. In addition, hydrogen generation rate versus catalyst concentration in the logarithmic scale was also plotted in the inset of Fig. 6b, from which we can see that the hydrolysis rate of AB shows a nearly linear relationship to the catalyst concentration. The slope of the line is 0.97 (close to 1.0), indicating that the hydrolysis of AB is first-order reaction with respect to the Ni/CNTs catalyst concentration.

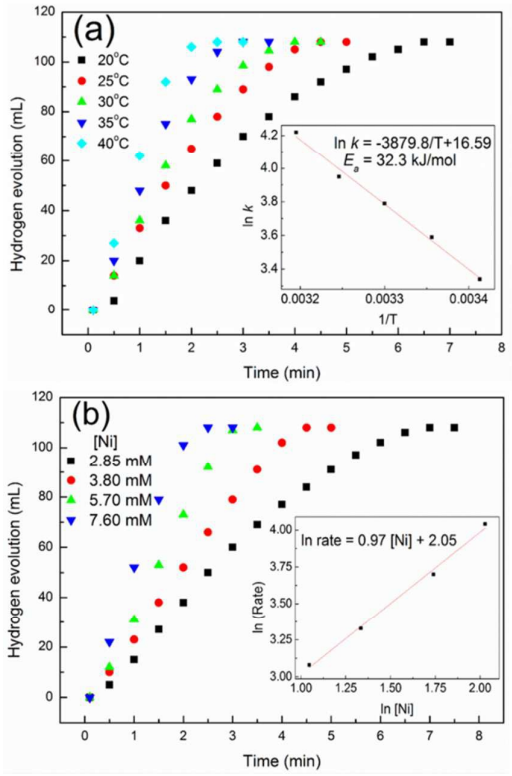

Fig. 6 Hydrogen generation from AB solution (0.15 mol/L, 10.0 mL) catalyzed by Ni/CNTs (3.8 mmol/L) (a) at different temperatures (inset: the corresponding Arrhenius plot of ln *k* vs 1/*T*) and (b) at different catalyst concentrations at 25 ± 0.5 °C (inset: the corresponding plot of ln rate vs ln [Ni]).

3.3 Promotion effect of Pt doping on Ni/CNTs catalytic activity

Previous research has proven that noble metal Pt shows the highest catalytic activity and has nearly no induction time toward AB hydrolysis.[8, 23] The doping of a small amount of noble metal Pt may reduce the induction time and correspondingly enhance their catalytic activity and stability of non-noble Ni/CNTs nanocatalysts. To verify this, 0.68 wt% Pt (only 2 ALD cycles) was doped in Ni/CNTs nanocatalysts by ALD, i.e., Pt was first deposited onto CNTs followed by NiO deposition, and the effect of Pt doping on the catalytic performance for AB hydrolysis was also investigated. Fig. 7 shows the H_2 generation as a function of reaction time using Ni/CNTs and Pt-promoted Pt-Ni bimetallic nanocatalysts. The as-prepared NiO/CNTs has no activity in 0.5 h and even 1 h (not shown) because it is generally considered that low valence states of the transition metals are active phases for the hydrogen evolution in the present reaction. However, with the as-prepared Pt-promoted Pt-NiO bimetallic nanocatalysts, hydrogen evolution was observed and the reaction was completed in 12 min. As expected, the catalytic activity of obtained Pt-Ni/CNTs bimetallic nanocatalysts reduced by H_2 at 325 °C has a further enhancement in comparison with monometallic Ni/CNTs. The reaction was completed only in 2 min without induction time. Data comparison of Ni/CNTs nanocatalysts before and after Pt doping was summarized in table S2.

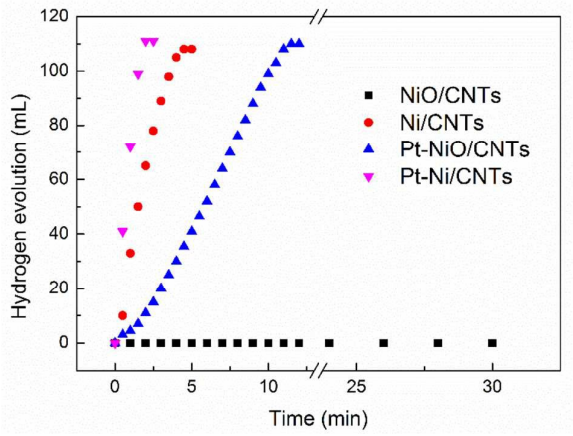

Fig. 7 Hydrogen generation from AB solution (0.15 mol/L, 10.0 mL) at 25 ± 0.5 °C catalyzed by nickel based nanocatalysts before and after Pt doping.

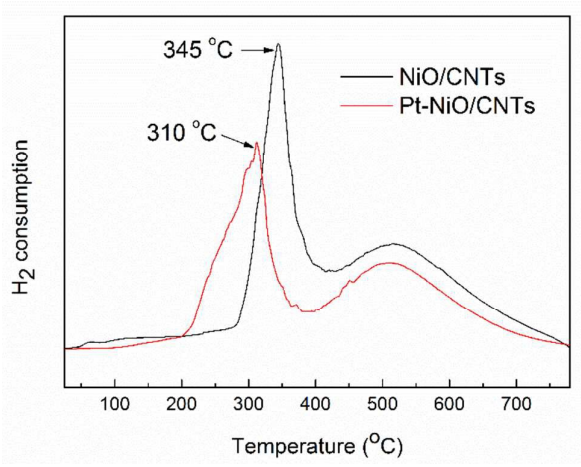

Fig. 8 H_2-TPR profiles of NiO/CNTs and Pt-NiO/CNTs catalysts.

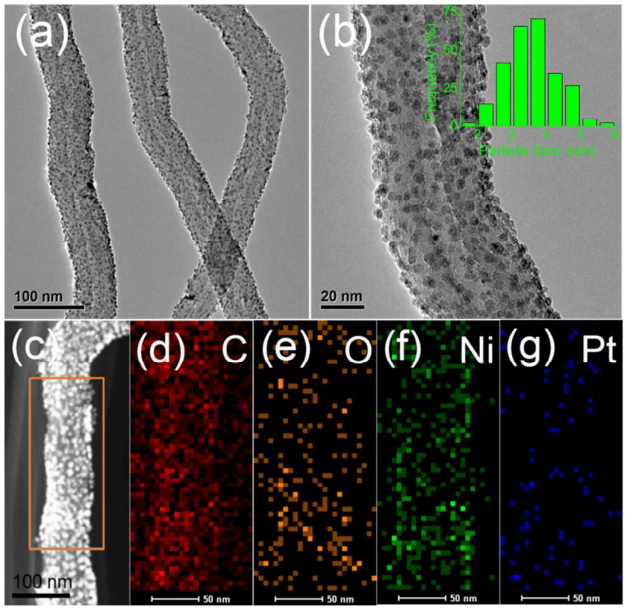

Fig. 9 Low (a) and high magnification (b) TEM and HAADF-STEM (c) images of bimetallic Pt-Ni/CNTs catalysts obtained by H_2 reduction at 325 ^{o}C (inset in Fig. 9b: the corresponding histograms of particle size distribution of the catalysts). Elemental maps of the rectangle area in (c) for carbon (d), oxygen (e), nickel (f) and platinum (g).

Synergistic effect between the two metals and smaller NPs may account for the enhanced catalytic activity of Pt-Ni/CNTs bimetallic nanocatalysts.[41, 42] Fig. 8 gives the TPR profile of NiO/CNTs and Pt-NiO/CNTs catalysts. During the reduction in the NiO/CNTs, there is narrow hydrogen consumption peak at around 345 ^{o}C. This peak is typically attributed to reduction of NiO to Ni, which has relatively weak interaction with CNT support. The second broad peaks ranging from 400-650 ^{o}C (centered at 500 ^{o}C) is mainly assigned to hydrogenation of the surface oxygen-containing groups of carbon materials including CNTs and the reduction of hard-to reduce Ni^{2+} species that have a strong interaction with CNT support.[42] Obviously, the first hydrogen consumption peak decreases from around 345 ^{o}C to 310 ^{o}C after only 2 ALD cycle Pt doping, i.e., Pt-NiO/CNTs bimetallic nanocatalysts are easier to be reduced compared with monometallic NiO/CNTs nanocatalysts, which is due to the easy dissociaticon of molecular hydrogen chemisorbed on Pt as atomic hydrogen, followed by spillover of hydrogen to NiO.[42] H_2 spillover effect may result in the simultaneous and easy reduction of NiO at lower temperature.

Fig. 9a-c show TEM and HAADF-STEM images of bimetallic Pt-Ni/CNTs catalysts respectively, indicating a uniform dispersion of discrete Pt-Ni NPs on the CNTs. EDX maps of carbon, oxygen, nickel and platinum are also given in Fig. 9d-g, which further proves the uniform distribution of Ni and Pt element on CNTs. The average size of the NPs is about 3.6 nm, which is smaller than that of Ni/CNTs (5.6 nm). Even if the bimetallic nanocatalysts were reduced at higher temperature (375 ^{o}C), nearly no decrease was observed in view of the catalytic activity (Fig. S4). Furthermore, the durability of Pt-Ni bimetallic catalysts improves remarkably in comparison with monometallic Ni/CNTs (Fig. S5). For the Pt-Ni bimetallic catalysts, the catalysts still preserve about 50% of their initial catalytic activity after the sixth cycle with complete conversion of AB, while the Ni/CNTs catalysts only preserve about 32% of their initial catalytic activity after the third cycle. Overall, 0.68 wt% Pt doping not only enhances catalytic activity of Ni/CNTs but also improves their durability. This is probably due to the lower reduction temperature needed for bimetallic Pt-NiO/CNTs catalysts inhibits the growth/aggregation of nanoparticles, and thus the particle size decreases correspondingly. Smaller nanoparticles tend to have stronger interaction with CNT supports, which inhibits the aggregation and leaching of nanoparticles from support, leading to the enhancement of the catalytic activity and stability.[45] Further work on the mechanism of mutual promotion or synergistic effect between the two metals leading to the enhancement of the catalytic activity and stability of the Pt doped Pt-Ni/CNTs bimetallic nanocatalysts for hydrogen generation from AB is underway and the relevant work will be published in the near future.

4. Conclusions

In summary, we have successfully synthesized nickel nanoparticles deposited on CNTs with uniform dispersion and narrow size distribution by ALD. The results show that Ni/CNTs nanocatalysts produced with 200 ALD cycles, corresponding to average Ni nanoparticle size of 5.6 nm, have the best catalytic activity among all the Ni/CNTs nanocatalysts prepared in this work, i.e., affording a high TOF value of 26.2 $mol_{H2}\cdot mol_{Ni}^{-1}\cdot min^{-1}$ or hydrogen release rate of 10720.9 $mL\cdot min^{-1}\cdot g^{-1}$. The kinetic studies on these Ni/CNTs catalysts reveal that the catalytic hydrolysis of AB is first-order with respect to the catalyst concentration and the activation energy for the hydrolysis reaction is 32.3 $kJ\cdot mol^{-1}$. The activity and durability of Ni/CNTs nanocatalysts can be further enhanced by just doping 0.68 wt% Pt because of the promotion/synergistic effect between the two metals Overall, ALD may provide an alternative approach to non-noble catalysts for future development of AB into a practical hydrogen storage material for renewable energy applications.

Acknowledgements

This work was financially supported by the National Natural Science Foundation of China (21203229, 21173248 and 21403272), the Hundred Talent Program of the Chinese Academy of Sciences, the Hundred Talent Program of Shanxi Province, Youth Innovation Promotion Association of the Chinese Academy of Sciences, and Natural Science Foundation of Shanxi Province (2014011012-1).

Notes and references

1. U. B. Demirci and P. Miele, *Phys. Chem. Chem. Phys.*, 2014, **16**, 6872-6885.
2. J. Du, F. Cheng, M. Si, J. Liang, Z. Tao and J. Chen, *Int. J. Hydrogen Energy*, 2013, **38**, 5768-5774.
3. P. Z. Li, A. Aijaz and Q. Xu, *Angew. Chem. Int. Ed.*, 2012, **51**, 6753-6756.
4. M. Zahmakiran and S. Özkar, *Top. Catal.,* 2013, **56**, 1171-1183.
5. D. Sun, V. Mazumder, Ö. Metin and S. Sun, *ACS Nano*, 2011, **5**, 6458-6464.
6. Y. Li, P. Song, J. Zheng and X. Li, *Chem. Eur. J.*, 2010, **16**, 10887-10892.
7. L. Yang, N. Cao, C. Du, H. Dai, K. Hu, W. Luo and G. Cheng, *Mater. Lett.*, 2014, **115**, 113-116.
8. W. Chen, J. Ji, X. Duan, G. Qian, P. Li, X. Zhou, D. Chen and W. Yuan, *Chem. Commun.*, 2014, **50**, 2142-2144.
9. M. Yadav and Q. Xu, *Energy Environ. Sci.*, 2012, **5**, 9698-9725.
10. S.-K. Kim, W.-S. Han, T.-J. Kim, T.-Y. Kim, S. W. Nam, M. Mitoraj, Ł. Piekoś, A. Michalak, S.-J. Hwang and S. O. Kang, *J. Am. Chem. Soc.*, 2010, **132**, 9954-9955.
11. M. Chandra and Q. Xu, *J. Power Sources*, 2007, **168**, 135-142.
12. Q.-L. Zhu, J. Li and Q. Xu, *J. Am. Chem. Soc.*, 2013, **135**, 10210-10213.
13. J. Li, Q.-L. Zhu and Q. Xu, *Catal. Sci. Technol.*, 2015, **5**, 525-530.
14. C.-Y. Cao, C.-Q. Chen, W. Li, W.-G. Song and W. Cai, *ChemSusChem*, 2010, **3**, 1241-1244.
15. P. Z. Li, K. Aranishi and Q. Xu, *Chem. Commun.*, 2012, **48**, 3173-3175.
16. O. Ozay, N. Aktas, E. Inger and N. Sahiner, *Int. J. Hydrogen Energy*, 2011, **36**, 1998-2006.

17. Ö. Metin, S. Ö zkar and S. Sun, *Nano Res.*, 2010, **3**, 676-684.
18. Ö. Metin, V. Mazumder, S. Özkar and S. Sun, *J. Am. Chem. Soc.*, 2010, **132**, 1468-1469.
19. J. M. Yan, X. B. Zhang, S. Han, H. Shioyama and Q. Xu, *Inorg. Chem.*, 2009, **48**, 7389-7393.
20. T. Umegaki, J. M. Yan, X. B. Zhang, H. Shioyama, N. Kuriyama and Q. Xu, *Int. J. Hydrogen Energy*, 2009, **34**, 3816-3822.
21. T. Umegaki, J. M. Yan, X. B. Zhang, H. Shioyama, N. Kuriyama and Q. Xu, *J. Power Sources*, 2009, **191**, 209-216.
22. Q. Xu and M. Chandra, *J. Power Sources*, 2006, **163**, 364-370.
23. W. Chen, J. Ji, X. Feng, X. Duan, G. Qian, P. Li, X. Zhou, D. Chen and W. Yuan, *J. Am. Chem. Soc.*, 2014, **136**, 16736-16739.
24. Q. Zhang, W. Deng and Y. Wang, *Chem. Commun.*, 2011, **47**, 9275-9292.
25. G. N. Parsons, S. M. George and M. Knez, *MRS Bull.*, 2011, **36**, 865-871.
26. B. J. O'Neill, D. H. K. Jackson, J. Lee, C. Canlas, P. C. Stair, C. L. Marshall, J. W. Elam, T. F. Kuech, J. A. Dumesic and G. W. Huber, *ACS Catal.*, 2015, **5**, 1804-1825.
27. J. Lu, K.-B. Low, Y. Lei, J. A. Libera, A. Nicholls, P. C. Stair and J. W. Elam, *Nat. Commun.*, 2014, **5**, 3264.
28. J. Lu, J. W. Elam and P. C. Stair, *Acc. Chem. Res.*, 2013, **46**, 1806-1815.
29. A. C. Johansson, J. V. Larsen, M. A. Verheijen, K. B. Haugshoj, H. F. Clausen, W. M. M. Kessels, L. H. Christensen and E. V. Thomsen, *J. Catal.*, 2014, **311**, 481-486.
30. Y. Lei, B. Liu, J. Lu, R. J. Lobo-Lapidus, T. Wu, H. Feng, X. Xia, A. U. Mane, J. A. Libera, J. P. Greeley, J. T. Miller and J. W. Elam, *Chem. Mater.*, 2012, **24**, 3525-3533.
31. H. Feng, J. W. Elam, J. A. Libera, W. Setthapun and P. C. Stair, *Chem. Mater.*, 2010, **22**, 3133-3142.
32. H. Feng, J. A. Libera, P. C. Stair, J. T. Miller and J. W. Elam, *ACS Catal.*, 2011, **1**, 665-673.
33. Y. Lei, J. Lu, X. Luo, T. Wu, P. Du, X. Zhang, Y. Ren, J. Wen, D. J. Miller, J. T. Miller, Y. K. Sun, J. W. Elam and K. Amine, *Nano lett.*, 2013, **13**, 4182-4189.
34. Z. Gao, M. Dong, G. Wang, P. Sheng, Z. Wu, H. Yang, B. Zhang, G. Wang, J. Wang and Y. Qin, *Angew. Chem. Int. Ed.*, 2015, **54**, 9006-9010.
35. S. Akbayrak and S. Ozkar, *ACS Appl. Mater. Interfaces*, 2012, **4**, 6302-6310.
36. L. Zhou, T. Zhang, Z. Tao and J. Chen, *Nano Res.*, 2014, **7**, 774-781.
37. Y. Du, J. Su, W. Luo and G. Cheng, *ACS Appl. Mater. Interfaces*, 2015, **7**, 1031-1034.
38. V. Datsyuk, M. Kalyva, K. Papagelis, J. Parthenios, D. Tasis, A. Siokou, I. Kallitsis and C. Galiotis, *Carbon*, 2008, **46**, 833-840.
39. T. I. T. Okpalugo, P. Papakonstantinou, H. Murphy, J. McLaughlin and N. M. D. Brown, *Carbon*, 2005, **43**, 153-161.
40. X. Tong, Y. Qin, X. Guo, O. Moutanabbir, X. Ao, E. Pippel, L. Zhang and M. Knez, *Small*, 2012, **8**, 3390-3395.
41. Z.-H. Lu, H.-L. Jiang, M. Yadav, K. Aranishi and Q. Xu, *J. Mater. Chem.*, 2012, **22**, 5065-5071.
42. L. He, Y. Huang, A. Wang, Y. Liu, X. Liu, X. Chen, J. J. Delgado, X. Wang and T. Zhang, *J. Catal.*, 2013, **298**, 1-9.
43. L. Zhang, J. Zhao, M. Li, H. Ni, J. Zhang, X. Feng, Y. Ma, Q. Fan, X. Wang, Z. Hu and W. Huang, *New J. Chem.*, 2012, **36**, 1108-1113.
44. A. D. Taylor, Gregory J. DiLeo and K. Sun, *Appl. Catal. B: Environ.*, 2009, **93,** 126-133.
45. J. Wang, H. Tan, S. Yu, and K. Zhou, *ACS Catal.*, 2015, **5**, 2873-2881.

Table of Contents Graphic and Synopsis

Highly efficient Ni nanoparticles deposited on CNTs were synthesized by atomic layer deposition used for hydrogen generation from AB hydrolysis.